Geodetic Shear Strain Estimates from the 1906 Segment of the San Andreas Fault, California: Boxes, Models, and Results

Lewis E. Gilbert
Lamont-Doherty Earth Observatory,
Department of Geological Sciences, Columbia University
Palisades, NY

"*Has a dog Buddha-nature?*"

Introduction

In any scientific endeavor it is necessary to draw a box. The box separates that which will be considered from that which will be ignored. Consciously or unconsciously, this act is unavoidable; it is simply not possible to consider *everything*. Boxes can be literal as in the case of a geologic study where a field area has boundaries or they can be figurative as in the case of a literature review which concerns itself with a single topic. In the case of a review the box is a set of decisions concerning the relevance of associated topics to the one of interest.

The drawing of boxes is a reductionist act. Its validity is based upon the notion that no essential information is lost by dividing the whole into subsets; the whole is the sum of its parts. This is equivalent to the assumption that the system under consideration is linear. This must be true because after the little bits are understood the system must go back together again. The things that have been learned at the small scale must still be true and the bits must go together in a way that can be understood. They must add. If there are terms beyond additions, the cause and effect relationships which were learned from the reduced systems will interact in unexpected ways and we will have failed to learn much about the system as a whole. The choice of box is important; that choice determines what will be known.

This paper is concerned primarily with the contextual framework reflected in geodetic studies along the section of the San Andreas fault which broke in the great 1906 San Francisco earthquake. It has both geographic and conceptual boxes. My geographic boxes are illustrated in Figure 0. There are two levels of box in that figure. The limits of Figure 0 isolate the portion of the Pacific - North American plate boundary (Pac:Nam) which is dominated by strike-slip deformation from sections to the north and south which are dominated by convergence and divergence. The smaller box labeled "Study Area" separates the section of Pac:Nam which ruptured in the 1906 San Francisco earthquake from the remainder of the strike-slip portion. (Pac:Nam is another box; Figure 0 actually isolates the strike-slip portion of Pac:Nam from *everything* which is outside of Figure 0; similarly Study Area separates the region of the 1906 break from *everything* which is beyond Study Area.) The conceptual box that I have settled on separates ideas and

results related to post-seismic movements from all other ideas and results related to the earthquake cycle.

The boxes I have chosen are arbitrary to varying degrees. Study Area is defined by the 1906 break and my conceptual box is defined by considerations of the amount of related information and my perceptions of divisions within the literature. The boundaries that I have chosen do not exclude influences from beyond the boundaries, they only shield my eyes from them. There are no guarantees that deformations within my box will have their cause completely enclosed by Study Area. In fact it is easy to imagine that the opposite is more likely to be true. Especially at the boundaries, it is just as likely that causes come from beyond the box as from within it; thus my hopes of understanding the shear portion of Pac:Nam by concentrating only on Study Area must be limited. Just as the character of the fracture fabric enclosed by the limits of Figure 0 is the result of the migration of triple junctions which are beyond its boundaries, the history of Study Area is influenced by the evolution of the creeping section to the south and the Mendicino area to the north.

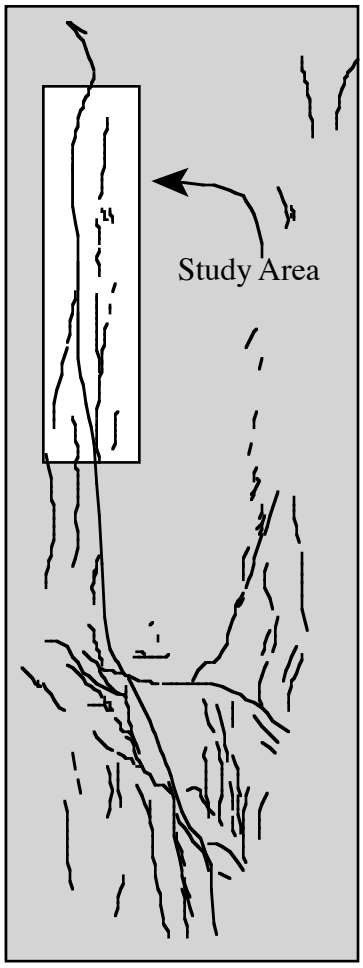

Figure 0: A map of the fracture fabric of Pac:Nam. Shown here, the fractures are plotted in an oblique Mercator projection about the NUVEL-1 pole of rotation for the Pacific and North American Plates.

Study Area became a natural box on 18 Apr 1906 (or was it 21 Oct 1868?). On the 18th the destruction of San Francisco was initiated by a great earthquake and it is the surface extent of the rupture associated with that event which defines the long axis of the box. The across axis dimension is defined by the lack of land on the west and the lack of geodetic data on the east. The earthquake disturbed the local geodetic network and the geodesists responsible for the maintenance of geodetic control realized that portions of the network would have to be resurveyed. Andrew Lawson, chairman of the State Earthquake Commission, recognized the magnitude of the problem confronting San Francisco and called for "deliberate investigation extending through years and decades and conducted on a wisely planned program" (Lawson 1908, p.151). Based in part upon the results of the resurvey, Reid (1910) proposed his now famous elastic rebound theory. The shock of 1906 did get an ongoing geodetic effort in the San Francisco region started; how deliberate and planned it was is open to debate. The area is littered with geodetic networks which have histories with a variety of temporal and

spatial ranges and data types. In the following paragraphs the networks considered in this review (Figure 1) will be described; it must be noted at this point that each network is a smaller box within Study Area.

The Networks

Hollister

This network straddles the intersection of the San Andreas fault (SAF) and the Calaveras fault at the southernmost end of the 1906 rupture; south of this network the relative motion between the Pacific and North America is relieved by steady state creep. The network has been monitored with triangulation sporadically since the 1906 event. Using the available triangulation data Scholz and Fitch (1969) published the first post-plate tectonic analysis of that data. Those authors concluded that strain accumulation in this network was homogeneous and accumulating. This conclusion drew harsh criticism from Savage and Burford (1971) . Savage and Burford wrote two papers (in addition to their criticism of Scholz and Fitch) concerning this network. Their first paper (Savage and Burford 1970) concluded that motion associated with Pac:Nam was taken up as block sliding across the SAF with little or no associated elastic strain accumulation; this paper established the plate tectonic oceanic transform model for the SAF. In their 1973 paper, Savage and Burford calculate a relative plate velocity of 32 ± 5 mm/yr for Pac:Nam motion. They arrived at this value using both triangulation data from the National Geodetic Survey (NGS) and trilateration data from the California Department of Water Resources (CDWR). This network is again addressed by Savage and his colleagues at the U.S. Geological Survey (USGS) in 1979 (Savage et al. 1979) . In this paper block motion across the SAF (13±2 mm/yr) and Calaveras (17±2 mm/yr) is still the dominant mode of deformation but improvements in data quality now allow the identification of some strain accumulation. The strain accumulation is principally in the block between the faults, but accumulation to the east of the Calaveras is also noted. The authors detected no strain accumulation west of the SAF. The velocity results of Lisowski et al. (1991) reiterate this picture and illustrate more clearly the block between the Calaveras and SAF is probably undergoing some internal deformation.

South Bay and East Bay

The next network to the north is the South Bay network of Prescott et al. (1981) . The South Bay and East Bay networks are subsets of a larger network used to monitor deformation south of San Francisco. The division of the larger network into subsets reflects the increasing complexity of the deformation field. The South Bay network spans the SAF and the intersection of the Hayward and Calaveras faults. In this area, both the Hayward and Calaveras are slipping at about 7 mm/yr and the SAF appears to be locked at the surface (Prescott et al. 1981) . West of the Hayward strain is accumulating over a broad region which extends to the west of the SAF (Prescott et al. 1981; Lisowski et al. 1991) . East of the Calaveras very little strain is accumulating. Prescott et al.

(1981) report that the South Bay network east of the Calaveras is rotating clockwise relative to the rest of the network; however, Lisowski et al. (1991) make no mention of such rotation and it is not apparent in the their results. Displacement rate across the South Bay network is reported to be 32.1± 7.4 mm/yr (Prescott et al. 1981) . Lisowski et al. (1991) report 31.0 ± 1.6 mm/yr for the combination of the South Bay and Hayward

Figure 1: Index map for networks within Study Area. Triangles labled with smaller face are stations mentioned in the text and mark the corners of the Primary Arc.

networks.

In the East Bay, the Hayward fault slips at 6.8 ± 1 mm/yr. The Calaveras may be locked at very shallow depths but below a few kilometers it also slips at 6.8±0.7 mm/yr. Data from the Calaveras Lake network indicate about 2.5 mm/yr slip at the surface across the Calaveras. It is possible that no elastic strain is accumulating with the East Bay (Prescott et al. 1981) .

San Francisco Peninsula

This area is not covered by a specific regional network but results from SAF crossing nets at Black Mtn. and Lake San Andreas and the Radio Facility network west of the SAF indicate that strain is accumulating along the peninsula. Slip rates above 1.5 mm/yr are ruled out by the data (Prescott et al. 1981) .

Hayward

The Hayward network is a densification of the Primary Arc (which will be discussed below) and it encloses much the same area as the East Bay network and the San Francisco peninsula. It is distinguished from those two by the fact that the former were observed with trilateration while this network is a triangulation network. Data from this network were collected in 1951, 1957 and 1963. Strain calculations from those data have been reported by Thatcher (1975) who finds roughly uniform strain over the network. The triangulation data suggest that the strain rate in this network has not been constant through time (Pope et al. 1966; Thatcher 1975) . Further evidence concerning this change is discussed in detail below.

North Bay

This region is not covered by a single coherent network; rather work north of the city has primarily been in the form of observations of smaller local networks. The oldest of these networks is the Point Reyes network. Originally this network was just the Point Reyes section (Figure 1). After the 1906 earthquake and as part of the effort to understand the distribution of strain away from the fault, several dense networks were installed along the fault (the Hayward Arc was also installed in this effort); thus in 1930 the Petaluma portion of the Point Reyes-Petaluma net was first observed. In addition to observations in 1930, the arc was observed in 1938 and 1961. The Point Reyes portion of this network was also observed immediately after the earthquake. Trilateration networks near Napa, Santa Rosa, and the Geysers have been observed since around 1970. For the purposes of this paper the networks at Fort Ross and Point Arena are included in the North Bay area. These two triangulation networks were first surveyed before the 1906 earthquake and were resurveyed immediately afterwards; however, they have not been extensively surveyed since. Fort Ross was remeasured in 1930 and 1969; Point Arena was remeasured in 1925 and 1930.

The major faults in this area include the SAF and the faults of the Rogers Creek system; these are roughly parallel. To the east, less well developed faults along the eastern edge of the Coast Ranges tend to strike more northerly than the SAF. Deformation in this region is distributed over a broad region. There is no indication of steady state slip across any of the faults and the strain is smoothly distributed (Prescott and Yu 1986) . Deformation in the Geysers net is dominated by strain associated with Pac:Nam but includes a component related to nearby geothermal activity.

Primary Arc

The Primary Arc is the network composed of the first order stations which were installed prior to the 1906 earthquake and which have been reobserved as many five times since their installation. In Figure 1 it is the polygon with vertices at Mocho, Sierra Morena, Tamalpais, Ross Mtn., Mt. St. Helena, Mt. Vaca and Diablo. It spans a region about 80 km wide and extends along the strike of the SAF from the Geyser network to the southern edge of the Hayward net (Figure 1). The area enclosed by this network includes the varied deformation styles south of San Francisco and the uniform broad field north of the city.

Data from the entire along-strike extent of this network has been used by Thatcher (1975; 1975) to constrain pre-, co- and post-seismic deformation (the paper concerned primarily with release (Thatcher 1975) uses data from as far south as Hollister). Thatcher does not include data from the stations Mt. Vaca or Mt. St. Helena in his deformation and instead uses observations to a station in the eastern most Point Reyes - Petaluma Arc.

Gilbert et al. (1992 in press) use data from the Primary Arc polygon which encloses the North Bay region and has vertices at Diablo, Tamalpais, Ross Mtn., Mt. St. Helena and Mt. Vaca. In addition to triangulation data, that paper presents results from a GPS resurvey. They refer to the region as their Coast Ranges polygon.

Shelter Cove

This network is at the northernmost extreme of both the 1906 rupture and the shear portion of Pac:Nam. This network was first observed in 1930 and reoccupied in 1976. Strain appears to homogeneous and parallel to the local expression of the SAF which strike N16W in this area (Snay and Cline 1980) .

Modelling

The job of the scientist is to make sense of the world. A common way to further this effort is to make analogies between things which are understood and those which are not. The analogy is often in the form of a physical model and we can *always* write:

$$\text{data} = \text{model} + \text{residual} \qquad (0$$

The terms in Eqn. 0 can be interpreted on a number of levels. At the most general level, data are observations, model is an analog to the processes being studied, and residual is

that which the model cannot explain. In this interpretation, the form of Eqn. 0 is slightly odd; one might expect something more like:

data - model = residual (0a

The form of Eqn. 0 was chosen to illustrate an often overlooked aspect of the observation process. When we collect data, we have in mind, consciously or unconsciously, a model of what we expect to find. It is that model which guides the experiment design process; we design experiments/measurements with expected results in mind. We do not design equipment to measure things which are not expected, but this does not mean that the unexpected would not be measured if it was looked for. In this way, what we actually do find is determined in large part by our expectations (Kuhn 1970) . In this abstraction of the data gathering process, residual is a nagging sense that something is not entirely right (see again Kuhn (1970)).

An individual model is identified by a set of equations whose free variables, the model parameters, take on specific values. A class of models is a set of models which are defined by the same equations, but whose model parameters are unspecified. A class of models (e.g., $y = ax + b$) is a subset of all the possible models, and an individual model (e.g., $a = 1$; $b = 0$) is a member of that subset.

As with boxes, models divide the world into two bits; the bit which the model explains (that which is understood) and the bit which the model fails to explain (that which is still a mystery). The objective in a modelling effort is to maximize the portion of the data which is understood and to minimize that which is not. To do this we look for model parameters which minimize the residual in Eqn. 0a. This is equivalent to choosing the member of a class of models which most resembles the data on hand. An unavoidable part of the modelling process is the selection of {selecting} the class of models from which the best representative will be chosen. If an inappropriate class of models is chosen, the best representative will still be an inadequate analog for the process being studied. Following this, another approach to minimizing residual is to choose another class of models; thus the modelling process has two levels: 1) selecting the class of models to be considered; and 2) choosing the best model from within the selected class. The multiple working hypothesis idea of Chamberlain (1897) implies that we should always use at least two classes of models in our attempts to understand our data. There is no guarantee that the "best" (meaning True) model is a member of *any* class of models.

Models which are interesting and add significantly to our understanding have far fewer adjustable parameters than there are data which need explaining. In such a situation the residual will always be finite and the possibility of finding a better model will always exist (Popper 1968; Hofstadter 1980) .

Meta-Models

There are many conceptual levels of models which range from philosophical discussions of perception to quantification of the rheology of plate boundaries. In this paper meta-models are conceptual frameworks which, on a day to day basis, operate on a sub-conscious level. They are often taken for granted and assumed without statement. A few models of this type which are of importance to geodetic studies are discussed briefly below.

Uniformitarianism

In Earth science the deterministic doctrine of western rationalism has historically taken the form of uniformitarianism. The basic tenet of uniformitarianism is that it is possible to understand the past by studying the present. In its strictest interpretation, rates and processes of the furthest reaches of the geologic history are the same as those of the present. Toward the looser end of the domain of this conceptual frame is the attitude that it is only the basic laws of physics which need not have changed through time. Uniformitarianism is a class of models; the adjustable parameters of this class take the form of the strictness of interpretation.

Homogeneity, Isotropy, Linearity, and Continuity

If questioned, most Earth scientists will readily admit that Earth is not a linear, homogeneous, isotropic anything; none-the-less, the linear, homogeneous, isotropic conceptual frame is present in almost all efforts at understanding Earth. It commonly enters shortly after the statement of a problem as assumptions which make it possible to write down and solve sets of equations which are models of Earth processes. If one pays close attention, these assumptions are often present even when they are not stated (e.g., the assumption that stress and strain are parallel is necessarily true only for an isotropic medium). The equations which we write down as analogs to Earth processes are invariably continuous. Even with simplifying assumptions, it is often necessary to discretize and approximate in order to arrive at a useful solution and despite the great success of such discrete models of Earth processes, we still believe that natural processes are ultimately continuous.

Elastic Rebound

This model explaining the recurrence of earthquakes is included in the meta-model category because of its dominance at a subconscious level. It was first formulated in the context of the normal faulting in the Great Basin by Gilbert (1884) , but is usually attributed to Reid (1910) who developed it in the context of the devastation associated with the 1906 San Francisco event. In this model, earthquakes are the rapid release of elastic strain which has accumulated slowly during an inter-event period. Variations within this model's domain are related to the source of the strain and the details of its accumulation. It is at the heart of all efforts directed toward understanding the earthquake cycle.

Plate Tectonics

Plate tectonics has been hailed as "the greatest geological discovery of our time" (Oliver 1987) and is the current guiding light in all but the fringes of geology and geophysics. As originally formulated (McKenzie and Parker 1967; Isacks et al. 1968) this model asserts that the surface of Earth is covered with a mosaic of rigid plates which deform only along their narrow boundaries. Among the great successes of plate tectonics is its explanation of the global distribution of earthquakes. In this model, earthquakes are the result of the interaction between two plates as they stick and slip past each other. Because plates are rigid and deform only along their boundaries, earthquakes can only occur at plate boundaries; thus the distribution of earthquakes actually *defines* the locus of plate boundaries. The energy released in earthquakes is the elastic strain which has accumulated due to friction (or some retarding mechanism) along the fault; the process which supplies the stored strain is the plate driving mechanism.

Plate tectonics was formulated in the context of the seafloor and its extension to continental problems replaced the continentally derived concept of geosynclines. Initially the boundaries of plate tectonics were thought to be single faults; however, recently the notion of narrow is being relaxed to include fault zones whose across-strike dimensions are similar to plate thicknesses. It is in the continents that the plate tectonic residual (wide boundaries and internal deformations) has been the greatest. Much of the difficulty associated with continental problems may be related to an improper model (Beloussov 1990) and as noted above, one way to reduce that residual may be to adopt a different class of models (Carey 1976) .

Models

Elastic Half-Space Models

In the plate tectonic model, Pac:Nam is a transform boundary and, in analogy to the ocean floor, the SAF is considered to be a transform fault (Savage and Burford 1970) . In geodetic studies which are concerned with the earthquake cycle, the most common model for such a boundary is a screw dislocation in an elastic half-space (Figure EM). (The popularity of this model warrants it having a name and I will call it 'EM'). EM captures the essence of strict plate tectonics; tectonic plates are represented by elastic half-spaces and the relative motion across a strike-slip boundary between two plates takes place across a single infinite planar discontinuity. Below some locking depth D, the plates move with the full plate velocity. Above D the plates are locked except for brief instants when there is an earthquake (Figure EM (a)). During an earthquake, the locked portion slips by the amount necessary for the surface portion to catch up with the freely slipping deeper portions. If V and t are the average velocity and the time since the last earthquake, then the amount of slip in the upper layer during the earthquake will be Vt. If earthquakes are periodic with a period T, then the slip in any earthquake will be VT.

In the long term average, the two plates slide past each other with no internal deformation (Figure EM (b)).

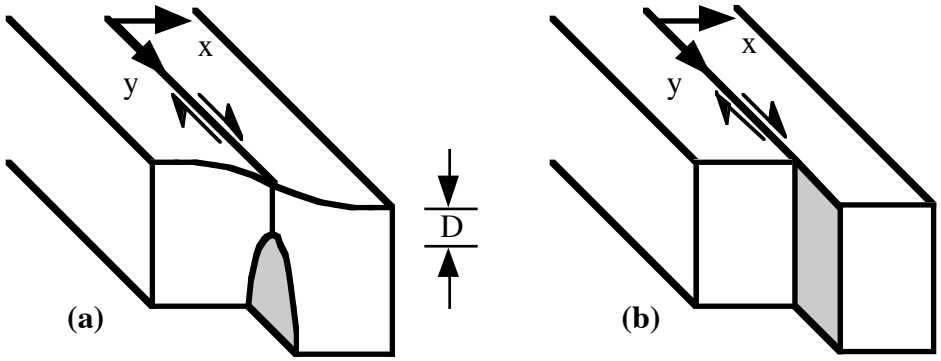

Figure EM: The figure published by Savage and Burford (1970) as a physical models for a plate boundary and the earthquake cycle.

The earthquake cycle deformation patterns possible in EM are strictly defined. For two plates locked to a depth D and moving with long term rate V, the fault parallel velocity along profile in the x direction is given by

$$v(x) = \frac{V}{\pi} \arctan\left(\frac{x}{D}\right) \qquad (1$$

and the fault parallel (maximum) engineering shear strain rate ($\dot{\gamma}$) is given by

$$\dot{\gamma}(x) = \frac{VD}{\pi (x^2 + D^2)} \qquad (2$$

(Figure EMP) (Savage and Burford 1973) . The adjustable parameters of EM are D, the locking depth, and V, the relative velocity of the two plates. EM is a subset of all of the possible deformation fields and its domain is spanned by all possible combinations of D and V.

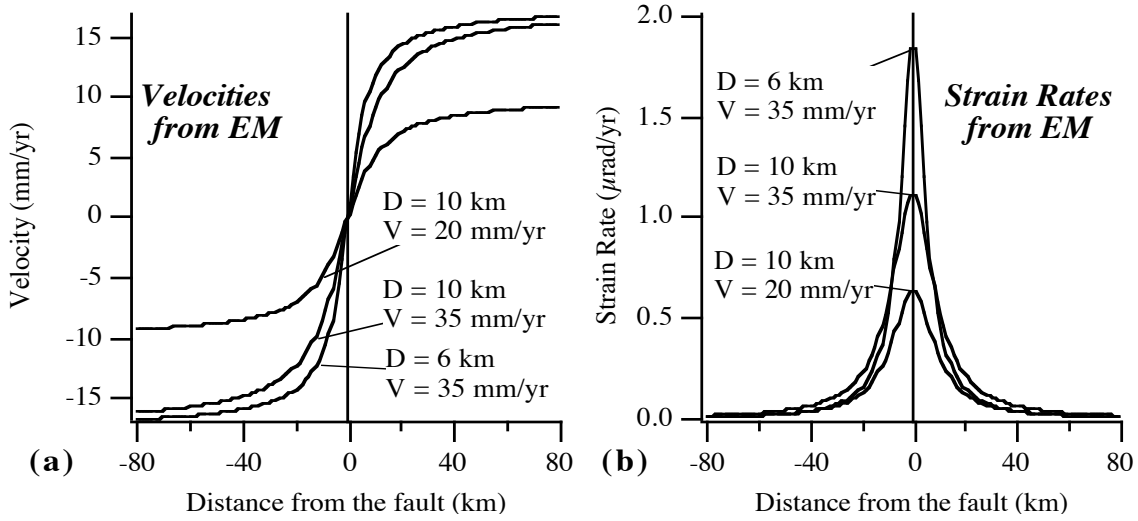

Figure EMP: a) Examples of velocity profiles of several members of EM. b) Examples of strain rate profiles of several members of EM.

While the formulation of EM is based on elastic half spaces, the surface deformations associated with EM are independent of the rheology at depths greater than D. Savage and Prescott (1978) investigated the effect of replacing the elastic half space with a system in which an elastic plate with thickness H overlies a viscoelastic substrate. They found that, for a sequence of greater than 10 periodic earthquakes, the surface deformation produced by the two systems is equivalent; thus within the conceptual frame of EM, surface observations of deformation cannot uniquely discriminate between elastic or viscoelastic behavior at depth.

As the business of Earth science returned to normal after the emergence of the plate tectonic paradigm, it became necessary to accommodate more and more of the relative motion of Pac:Nam on faults other than the SAF. As long as linearity is assumed, EM is easily extended to EM'. EM' has two or more parallel faults whose deformation fields add (Figure EM') (e.g. Prescott et al. (1979)). In EM' each fault has an associated D and V; thus if the placement of the faults is taken as fixed from the regional geology, the number of adjustable parameters in EM' is twice the number of faults. In the limit, EM' can be made to simulate a broad shear zone by letting the number of screw dislocations beneath the locked layer go to infinity and distributing those dislocations continuously over a finite region (Prescott and Nur 1981) .

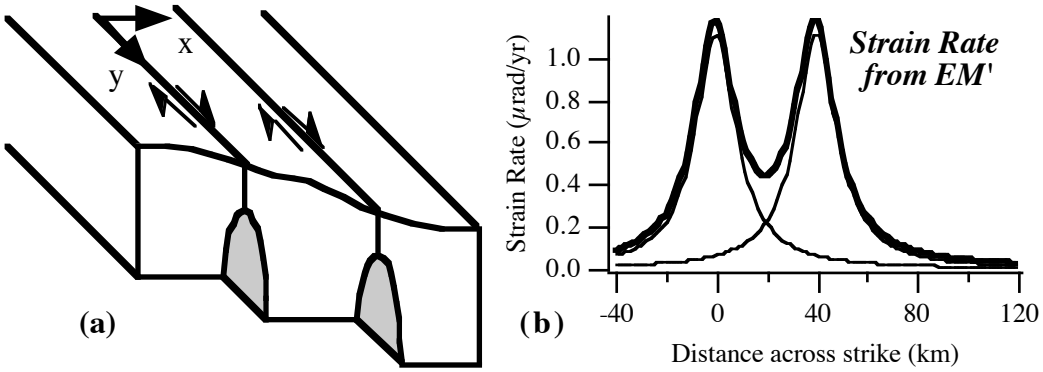

Figure EM': Model EM' illustrated. a) Schematic diagram of the model with two faults. b) Strain profiles for V = 35 mm/yr and D = 10 km on two faults separated by 40 km. The light lines are strain rates for single faults; the heavy line is the sum of the profiles for the single faults.

EM and EM' have been used extensively to describe observed deformations within Study Area. EM was first proposed in regards to studies in the Hollister network (Savage and Burford 1970; Savage and Burford 1973) . In 1973 Savage and Burford noted that if this model applies to a region, deformation will extend to considerable distance from the driving fault; to measure 90% of the attendant deformation it is necessary to extend observations to a distance of 6.3D from the fault. If D=15 km, it is necessary to consider an area which extends 95 km from the fault. If it can be assumed that the region is homogeneous with respect to the fault, only one side of the fault need be observed.

In their 1973 paper, Savage and Burford were trying to estimate the relative velocity across Pac:Nam from geodetic networks which extend only about 40 km from the fault and the breadth implicit in EM was of some concern. As noted above, the deformation in the Hollister network is dominated by steady state slip and after careful consideration, Savage and Burford decided that all of the deformation could be accounted for and presented their 32±5 mm/yr plate rate with confidence. In 1979, when Savage et al. (1979) returned their attention to the Hollister region, an elastic model which took into account the non-parallel fault geometry of the region and the creeping nature of portions of the upper layer was used to find values for D and V for the SAF and Calaveras which best characterized the deformation of the region. The values from their model vary, but their preferred model has values of ~9 mm/yr and ~23 mm/yr for slip at the surface and at depth for the SAF and ~15 mm/yr slip across the entire fault surface for the Calaveras north of the town of Hollister.

In the South Bay network, lack of strain east of the Calaveras and EM are used to rule out values of D less than 50 km for the Hayward and Calaveras faults; differences in calculated station velocities are used to constrain displacement rates across the SAF, Hayward and Calaveras to 12, 8, and 5 mm/yr respectively (Prescott et al. 1981) . In the

context of EM, strain observed west of the Hayward in South Bay must be caused by slip at depth on the SAF (Prescott et al. 1981) .

In the East Bay net, the Hayward fault is slipping throughout its depth at ~7 mm/yr; thus D = 0 km. Deformation associated with the Calaveras fault is a little more complicated. In addition to calculating strain rates for the entire East Bay net and for the Calaveras net, Prescott et al. (1981) calculated significantly higher strain rates from very short lines which just crossed the Calaveras fault. Using EM they reasoned that the rapid decrease in strain rate as the net size got larger constrained D to be very shallow and concluded that below 2-3 km the Calaveras slips at ~7 mm/yr. The upper layer appears to be slipping at about 2-3 mm/yr and it is proposed that the difference between the upper and lower rates is accommodated as anelastic deformation close to the fault.

Compared to the South Bay and East Bay networks, the San Francisco peninsula portion of the SAF is rather simple. Prescott et al. (1981) use the average strain rate from the Black Mtn/Radio Facility and Lake San Andreas, the displacement rate for the SAF in the South Bay network and Eqn. 2 with x = 0 to calculate a value of about 6.5 km for D.

In the North Bay, Prescott et al. (1979) used EM and strain rate estimates from the Point Reyes, Santa Rosa and Napa networks to constrain the values of D and V. In their paper the plate boundary was taken to be at the position of the SAF; the fault parallel component of deformation within the Napa network is quite small and constrained the maximum value for D. It was found that values of 14±5 km and 46±11 mm/yr for D and V characterized the best member of EM. Seven years later, the North Bay deformation field was much better known and Prescott and Yu (1986) conclude that its now obvious breadth is best explained by EM'. Two equally acceptable variants were proposed: 1) 3 faults distributed as the SAF, Rogers Creek and West Napa faults each accommodating one third of the displacement or 2) a continuous dislocation distribution between the SAF and the West. For both variants, the best fitting value of D was found to be 10 km.

Viscoelastic Models

It is not possible for EM to model temporal variations of velocity or strain rate during an earthquake cycle (Eqn. 1 and 2); thus any such variations in the behavior of Pac:Nam, such as those noted by Thatcher (1975; 1983) and Gilbert et al. (1992 in press) will turn up as residual in EM (Eqn. 0a). Within the strict EM frame, temporal variations of rate *cannot* be accommodated. If variations in rate are to be modeled, a new class of model must be considered.

To account for temporal variations models which include an effect analogous to a viscoelastic response to the sudden slip in the surface layer have been proposed as alternatives to EM. Thatcher (1983) considered the lithosphere-aesthenosphere model of Savage and Prescott (1978) and a model he called the modified elastic half space model

(MEM). In MEM, temporal variation of the rate of deformation is accomplished by allowing transient post-seismic slip at depths between D and D_0 along the boundary between the plates. He concluded (as did Savage and Prescott) that surface observations could not distinguish between MEM and a lithosphere-aesthenosphere model.

A thorough development the viscoelastic model (VEM) is presented by Li and Rice (1987) . In their development, stress is cycled between the elastic upper layer (lithosphere) and a viscoelastic lower layer (aesthenosphere) through shear tractions along the interface between the two. During the earthquake stress is transferred into the viscoelastic layer. As time passes after the earthquake, the viscoelastic layer relaxes. The relaxation is accommodated by elevating near fault strain rates during the immediate post-seismic period and by lateral migration of stress with causes the surface strain field to broaden with time.

In 1990, Savage (Savage 1990) presented the formulation of time varying slip distributions along the interface in EM which produce the same surface deformations as a relaxing viscoelastic layer. Examples of profiles possible in VEM are given in Figure VEM. Note that there is a point at which the strain rate remains constant throughout the cycle; toward the fault from this point strain rate decreases with time, away from the fault, strain rate increases. Savage's result is a valuable extension of Thatcher's MEM for it shows formally that as far as surface deformations are concerned, VEM and EM (or MEM) are isomorphic; they contain the same information and explanatory power.

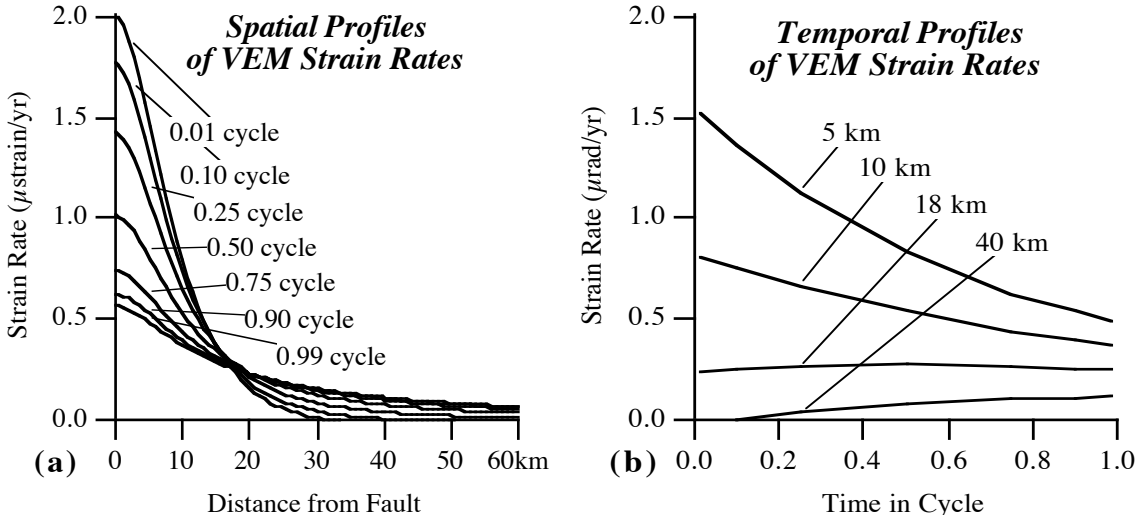

Figure VEM: Strain Rate profiles from Savage's (1990) order 2 formulation for VEM equivalent half-space slip distributions. For these profiles, locking depth = 10 km, full plate velocity = 35 mm/yr and $\mu T/\eta$ = 4. a) Profiles of fault parallel strain rate against distance from the fault for various times in the cycle. b) Profiles of fault parallel strain rate vs. time in the cycle for various distances from the fault.

Data, Results and Observations

Up until this point the terms, "data", "results" and "observations" have been used interchangeably. This reflects the fact that in the evolution of a field of study, the distinction between data, results and observations can become blurred. As work on a topic progresses, assumptions that were clearly stated in the beginning become taken for granted; they are no longer stated and exceptions to them are easily dismissed as mistakes. In an effort to see through the blurring, the following section presents some definitions and a discussion of data, results and observations in the context of the boxes of this study.

Definitions

Data

Data are things that are accepted as being facts; this is analogous to being accepted as independent of any model. It is this characteristic which makes data useful in constraining models. Unfortunately, as noted above, it is not possible for anything to be completely model independent; the very act of perception involves assumptions about what is likely to be seen. To accommodate this fact, data can be defined as things whose model we are willing to ignore or at least to accept without question. What is and is not data is a decision that is made in the context of the problem that is being considered. An example of something considered data in this study is the measurement of an angle between two triangulation monuments.

Results

Results are the output of some operation on data; results cannot be model free. Any sort of manipulation of data is done with some purpose and that purpose is determined by the choice of model. In the case of data reduction (e.g., averaging several measurements) the model is usually so widely accepted that the results are once again considered data. The fact remains that even averaging assumes something about the nature of the process which is being measured. An example of results in the context of this study is an estimate of shear strain rate calculated from changes in the angles between triangulation monuments.

Observations

Observations are generalizations from data or results and, like data, they are meant to be model free. Also like data, it is not possible for them to be so. Observations are the most pernicious of model hiders. It is in generalizing or expounding upon data or results that our preconceived notions are the most invisible. An observation in this paper is any statement concerning the nature of or implication of one or more estimates of shear strain.

Data

The 1906 segment of the SAF is unique in the length and detail of its geodetic history. Geodetic data were first collected in the region in the mid-1800's as the first transcontinental control network was installed. After the 1906 earthquake, geodesists realized that, in addition to providing local control for map making, their data could be used to monitor the deformation associated with the SAF. In fact monitoring such deformation was necessary in order to provide adequate local control; thus quasi-periodic measurements have been made in the region for over 100 years. In the time since the first measurements, the measurement technology has changed from triangulation to trilateration and in the last 5 years to satellite techniques that utilize the Global Positioning System (GPS). In the following sections each of these techniques is briefly described along with some of the assumptions that constitute the associated model.

Triangulation

This technique was the mainstay of geodesy until the mid-1960's. The measurement for this data type is an angle between permanent station monuments. Ideally all angles between all stations in a geodetic network are measured during a given measurement session (epoch). In addition to the angles between stations, the angle between a celestial body (commonly Polaris) and one or more stations within the network will be measured to gain external constraint on the network's orientation.

This technique assumes that light travels in a straight line between the observer and the monuments being observed. This is usually a reasonable assumption, but horizontal temperature gradients can cause refraction which will yield angle measurements which are misleading. Raw observations of angles must be corrected for differences in elevation between monuments. The height correction assumes that the geoid is adequately represented by an ellipsoid of revolution; thus the height correction for a given angle measurement includes a model of the geoid. The theodolite (the instrument for measuring the angles) is aligned with the geoid and not with the assumed ellipsoid; this requires another correction for the angle between the geoid and the assumed ellipsoid (deflection of the vertical).

Trilateration

With trilateration technique, distances rather than angles are measured. In modern trilateration, distance is measured by measuring the time it takes for a light pulse to travel from a source to a reflector at a distant station monument and back again. The speed of light is then used to convert the time into a distance. Such measurements are made between all (or at least most) stations with the geodetic network. This technique does not yield any information about the orientation of the network relative to any absolute frame of reference.

The speed of light is a function of the temperature and humidity of the air that it is travelling through; thus in order to convert the measured time into a distance,

corrections for these properties must be applied. In order to correct for them, temperature and humidity must be measured. This is commonly done in one of two ways: 1) end point measurements are made at the source and receiver; or 2) measurements are made with an aircraft which flies along the line as it is being measured. In both of these cases, assumptions about the structure of the atmosphere must be made; those assumptions constitute a model. In addition to corrections for the traveled path, corrections for differences in station heights and deflection of the vertical must also be applied and they bring with them their attendant models of the geoid and ellipsoid.

GPS

The measured quantity in GPS is the phase difference between a signal transmitted by a satellite and received at a geodetic marker and a similar signal generated inside of the receiver. This phase difference can be converted into a distance between the satellite and the monument. The measurements from several receivers recording signals from four or more satellites concurrently can be used to calculate both the satellite positions and the absolute vector differences between the positions of the receivers; however the calculations involved in transforming the measured phase differences into vector position differences are quite complex. GPS is a prime example of a technique where what is considered data (the vector position difference) is the result of several models. Some of those models include such things as the behavior of clocks, the effect of the ionosphere on electromagnetic radiation, and the structure of the troposphere (Leick 1990) .

Results and Observations

Calculations

It is in the calculation of results that assumptions of homogeneity and uniformity are most strongly represented. Even in "continuous" monitoring experiments, geodetic data are sampled at discrete times; no information about the time between measurements is known. Implicit in such a sampling scheme is that the sampling interval is small compared to variations which are likely to occur. Such an assumption reflects an a priori model of the process which is being studied. Generally it is necessary to assume that the process rate is constant, at least between individual measurements, and commonly it is assumed to be constant over a suite of measurements. Similar statements can be made about measurements which are distributed spatially. In this case, geodetic data reflect spatial averages of deformation and it is often assumed that the deformation is distributed homogeneously over the area being monitored. The uniformitarian idea that deformation should be distributed homogeneously in space and time is a deeply ingrained notion. Measurements which indicate departures from such a model are subjected to close scrutiny and are usually considered to be errors.

After primary geodetic measurements have been made and the appropriate corrections or processing have been applied, the data are ready for use. If measurements

have been made at only one time (one epoch), then the only thing which can be done is to find the station positions which best fit the measurements. This process is called "adjusting the data" and consists of finding the set of coordinates, within some reference frame, which minimizes the difference between the measurements which were actually made and those which would ideally be made from such positions.

If measurements have been made at more than one epoch, the geodetic data from the different measurement sessions can be compared to provide a measure of the amount of deformation. In studies prior to 1966, the quantity used to describe deformation was station displacement. To calculate station displacements, triangulation data from each epoch were adjusted independently and the resulting station positions were differenced. In adjusting data from Study Area, it was common to hold the length and orientation of the baseline between Mocho and Diablo (Figure 1) fixed in order to constrain the scale and orientation of the network. This line was held fixed because it was roughly parallel to the SAF and it was believed that it was at sufficient distance from the fault that it would undergo little deformation. In this sort of calculations, errors accumulate rapidly and strains were not normally calculated.

In 1966, Frank published a method for calculating shear strain directly from changes in observed angles (Frank 1966) . No information about orientation or scale changes can be found, but the shear strain of the region can be completely described by two shear strain parameters

$$\gamma_1 = \varepsilon_{22} - \varepsilon_{11}$$
$$\gamma_2 = \varepsilon_{12} + \varepsilon_{21} \qquad (3$$

where ε_{ij} are the principal strains oriented in a N and E reference frame (Figure G). In the region of this paper it is common to rotate the coordinate system so that γ_1 is parallel to the SAF. Frank's method assumes that the strain is homogeneously distributed between the stations which have been observed. Generalizations by Savage and Burford (1970) and Prescott (1976) of Frank's original formulation for complete triangles have made it the method of choice for papers using only triangulation data.

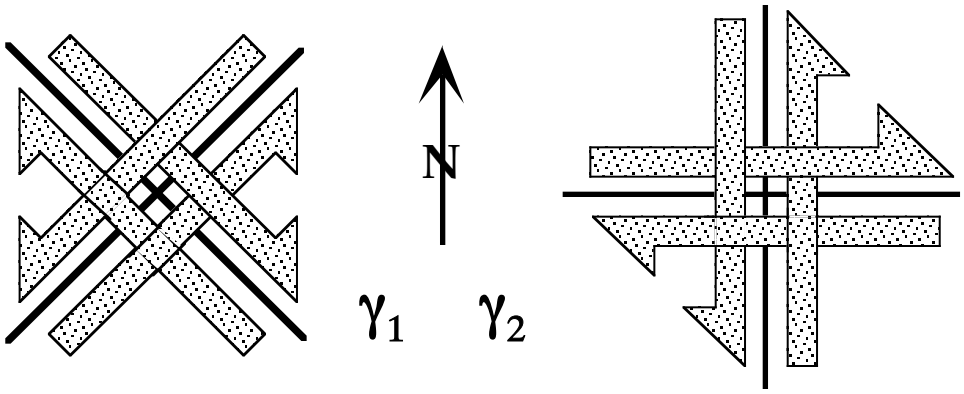

Figure G: The shear strain components. γ_1 represents right lateral shear strain across vertical planes oriented N45W and γ_2 represents left lateral shear strain across planes oriented N-S.

An equivalent representation of the shear strain uses the quantities γ, the magnitude of the maximum right lateral shear strain and ψ, the orientation of the plane across which that shear occurs. γ and ψ are used in this paper because they are easier to visualize and do not contain an implicit assumption that shear strain is always parallel to a constant direction. The magnitude of shear strain will depend upon the length of time between measurements; thus it is normal to assume that the rate of strain is constant between two measurement epochs and calculate a rate, $\dot{\gamma}$, by dividing the strain by the elapsed time between measurements. In using the result, the estimate is usually assigned at the midpoint between the two measurements.

With trilateration data the situation is a bit different. Lengths are being measured directly and the relationship to strain is more straightforward. Strain rates are generally calculated from the rate of change of lines whose length has been measured at several epochs. It is assumed that the rate of line length change for each line is constant and the uniform strain field which best produces the measured rate of line length change field is calculated.

In addition to strain, trilateration data can be used to calculate displacement and velocity fields. In such calculations there is an ambiguity associated with the possibility of rigid rotation and/or translation of the network. The translational ambiguity has little effect on the relative displacements of the stations within the network and is handled by holding some position within the network fixed; that position can either be an actual monument or the center of mass of the network. The rotational ambiguity is more bothersome. There are three ways to handle this problem: 1) fix the azimuth of a line within the network; 2) calculate a solution with no rotation about the center of mass of the network (the inner coordinate solution); or 3) calculate a solution which minimizes the component of displacement in some direction (the outer coordinate solution (Prescott 1981)). The outer coordinate solution was developed for the special case of a strike-slip environment. In that environment it is expected that displacements will be dominantly parallel to the faulting direction; if such a model is accurate, minimizing displacements

normal to the faulting direction is a reasonable thing to do. Any real displacement normal to the fault is anomalous in this model and will be suppressed. Lisowski et al. (1991) modify the outer coordinate solution and minimize motion normal to ψ. Their displacement calculation has two parts: 1) a uniform strain field for the data is calculated to get an estimate of ψ; and 2) the displacement field which minimizes motion normal to ψ is calculated.

Errors

It is not possible to measure anything without some doubt as to its actual value (which is not quite the same as having some doubt as to whether it has an actual value). The doubt comes about from the fact that measuring instruments and their operators have finite resolutions. In the collection of geodetic data errors come from several places. It is always necessary to set up the instrument over the monument for which data is to be collected. "Over the monument" means that the center of the measuring device is straight up from the center of the marker; errors associated with "straight up" and "center of the marker" can be minimized but will always be finite and hopefully random. Once the instruments have been placed, they must measure something and the exactness of the measurement is limited by the resolution of the measuring device. In triangulation, the limit is the gradation of the micrometer; in trilateration and GPS, resolution is limited by clock frequencies and the wavelength of the electromagnetic radiation being used (laser light in the case of trilateration, and microwaves in the case of GPS). Resolution in the GPS and trilateration cases is further limited by the processing which must be applied to the measured quantity in order to make the data useful. When all is said and done, triangulation has a resolution of about 1 part in 10^5, triangulation about 2 parts in 10^7 (Savage et al. 1981) , and GPS roughly 2 parts in 10^8 for horizontal components and 1 part in 10^7 for the vertical component (Larson and Agnew 1991) .

Errors in the data combine with idealizations in the models (e.g., assumptions about homogeneity) to produce results which also have some associated doubt. In the case of shear strains, we get $\dot{\gamma}_1 \pm \sigma_1$ rather than $\dot{\gamma}_1$ exactly. The same is true for $\dot{\gamma}_2$. $\dot{\gamma}$ and ψ are related to $\dot{\gamma}_1$ and $\dot{\gamma}_2$ by

$$\dot{\gamma} = (\gamma_1^2 + \gamma_2^2)^{\frac{1}{2}}$$
$$\psi = \frac{1}{2} \arctan\left(\frac{-\gamma_2}{\gamma_1}\right) \qquad (4$$

If $\dot{\gamma}$ and ψ are to be used to quantify the shear strain field, the errors associated with $\dot{\gamma}_1$ and $\dot{\gamma}_2$ must be propagated through Eqn.4. (Appendix 1).

Notice that $\dot{\gamma}$ will always be a positive value (Eqn. 4). This characteristic makes the error associated with $\dot{\gamma}$ a bit tricky. It is possible to imagine a scenario where non-zero estimates of $\dot{\gamma}_1$ and $\dot{\gamma}_2$ are due entirely to random error. Those measurements would combine through Eqn. 4 to produce a positive non-zero value for $\dot{\gamma}$. In this scenario the average of a large number of estimates of $\dot{\gamma}_1$ and $\dot{\gamma}_2$ will approach zero, but the average

of $\dot{\gamma}$ from those same estimates will always be positive and non-zero even though it is the result of a process whose real value is zero. When $\dot{\gamma}$ is considered below it will be plotted relative to a boundary which is the 95% confidence level of the hypothesis that it is the result of noisy measurements about zero mean process (Appendix 2). If $\dot{\gamma}$ is above that limit, we are confident that is reflects some active shear strain; if it falls below that limit, the level of strain is not known.

Results from the literature

Geodetic shear strain rate results from the 1906 segment have been compiled from the literature and they are presented in Table T.

Table T: A compilation of Shear Strain rate results from the literature.

Years		$\dot{\gamma}$	ψ	Location
1922	1929	0.55 ± 0.63	-20.84 ± 53.69	Coast Ranges
1929	1948	1.00 ± 0.43	-31.69 ± 11.83	Coast Ranges
1948	1963	1.37 ± 0.75	20.36 ± 7.82	Coast Ranges
1963	1991	0.41 ± 0.09	-28.67 ± 11.42	Coast Ranges
1906	1930	3.15 ± 0.61	-16.21 ± 6.16	Point Arena
1906	1925	2.27 ± 0.50	-17.74 ± 5.87	Point Arena
1925	1930	16.77 ± 7.93	30.77 ± 4.97	Point Arena
1906	1969	0.91 ± 0.08	-38.80 ± 2.54	Fort Ross
1906	1930	2.41 ± 0.80	-33.09 ± 8.20	Fort Ross
1930	1969	0.31 ± 1.08	-40.65 ± 59.81	Fort Ross
1930	1938	2.21 ± 0.73	-32.79 ± 9.97	Point Reyes
1938	1961	0.56 ± 0.16	-37.55 ± 8.93	Point Reyes
1930	1961	0.89 ± 0.18	-48.28 ± 6.54	Point Reyes
1906	1922	0.79 ± 0.20	-40.87 ± 9.60	Primary Arc
1922	1947	0.45 ± 0.17	-35.06 ± 10.82	Primary Arc
1907	1922	0.79 ± 0.23	-41.00 ± 10.00	Primary Arc
1922	1948	0.46 ± 0.17	-36.00 ± 13.00	Primary Arc
1951	1957	1.02 ± 0.39	-21.00 ± 16.00	Hayward Net
1957	1963	0.55 ± 0.25	-13.00 ± 18.00	Hayward Net
1951	1963	0.72 ± 0.13	-18.00 ± 8.00	Hayward Net
1930	1938	0.63 ± 0.39	-43.00 ± 19.00	Point Reyes - Petaluma
1938	1961	0.34 ± 0.08	-38.00 ± 8.00	Point Reyes - Petaluma
1930	1961	0.38 ± 0.10	-43.00 ± 8.00	Point Reyes - Petaluma
1972	1977	0.48 ± 0.05	-31.00 ± 3.00	Geyser
1972	1976	0.33 ± 0.10	-43.00 ± 9.00	Santa Rosa
1972	1976	0.73 ± 0.25	-35.00 ± 8.00	Point Reyes
1970	1976	0.17 ± 0.03	-8.00 ± 5.00	Napa
1970	1978	0.47 ± 0.02	-27.00 ± 2.00	SF Bay
1970	1978	0.38 ± 0.04	-26.00 ± 3.00	East Bay
1970	1978	0.48 ± 0.04	-36.00 ± 4.00	West Bay
1970	1978	0.73 ± 0.04	-26.00 ± 2.00	South Bay
1973	1978	0.13 ± 0.06	7.00 ± 12.00	Mocho
1973	1978	0.25 ± 0.06	-49.00 ± 80.00	Parajo
1971	1978	0.31 ± 0.04	-60.00 ± 4.00	Hollister - east of Calaveras
1970	1975	0.22 ± 0.14	-17.00 ± 18.00	Gavilan
1971	1978	0.32 ± 0.04	-61.00 ± 3.00	Eastern Block
1971	1978	0.66 ± 0.08	-53.00 ± 3.00	Central Block

1971	1978	1.24 ± 0.01	-33.00 ±	1.00	Whole Net
1930	1976	1.01 ± 0.18	-13.20 ±	4.50	Shelter Cove
1970	1980	0.33 ± 0.04	-48.00 ±	5.00	West of Hayward Fault
1970	1980	0.12 ± 0.02	6.00 ±	8.00	East of Calaveras
1970	1980	0.62 ± 0.07	-25.00 ±	4.00	Calaveras reservoir network
1970	1980	0.26 ± 0.02	-35.00 ±	4.00	Whole East Bay Network
1970	1980	0.61 ± 0.19	-28.00 ±	10.00	Lake San Andreas Net
1970	1980	0.56 ± 0.09	-52.00 ±	6.00	Black Mtn Net
1970	1980	0.80 ± 0.18	-47.00 ±	6.00	Radio Facility Net
1970	1980	0.58 ± 0.07	-47.00 ±	9.00	Average for San Francisco Peninsula
1960	1967	0.87 ± 0.10	-24.00 ±	4.00	CDWR network - East Bay
1970	1980	0.42 ± 0.02	-26.00 ±	2.00	CDWR network - East Bay
1972	1983	0.64 ± 0.07	-43.10 ±	2.30	Point Reyes
1972	1983	0.32 ± 0.02	-32.90 ±	1.90	Santa Rosa
1972	1983	0.39 ± 0.03	-34.00 ±	2.90	Geyser
1972	1983	0.17 ± 0.05	-25.00 ±	9.10	Napa
1973	1989	0.34 ± 0.02	-34.40 ±	1.50	North Bay
1973	1989	0.38 ± 0.02	-31.00 ±	1.60	South and Central (Hayward net)
1973	1989	1.15 ± 0.04	-36.00 ±	0.90	Monterey Bay (Hollister)

Boxes; slight return

Another function of boxes is to keep apples and oranges separate, and in this spirit, subsets have been compiled from the results of Table T. First order boxes are geographical. As noted above, the nature of the deformation field evolves from a narrow (~1km) zone of steady state creep in the south near Hollister, through a mixture of creeping and locked faults south of San Francisco, to a broad (~100 km) deforming zone with no creep north of the city. In compiling records of the temporal evolution it is important to avoid biases which could be introduced by spatial variability; thus the available results have been divided along the lines just outlined. The area north of the city (roughly the North Bay) is referred to as the Central 1906 segment (Figure 1) and the area to the south of the city is referred to as the Hayward net (Figure 1). Shear strain rates in the Hollister area are dominated by slip across the SAF and Calaveras; beyond that observation, results from that net have not been considered further.

Second order boxes are based on scale. Networks come in two sizes; large and small. Large networks span more than one fault. By this definition results from the Primary Arc and Hayward networks are large networks. Small networks are those which span only one fault or have an aperture on the order of 10's of km or less. These networks can be close to the SAF (Shelter Cove, Point Arena, Fort Ross, Point Reyes) or at some distance from it (Geyser, Santa Rosa, Napa). Despite the definition of the Central 1906 box, results from Shelter Cove are considered within that box. It should be kept in mind that Shelter Cove is at the northern extreme of the 1906 rupture.

Central 1906 Segment

Results from the Central 1906 segment (Figure 1) are compiled in Table Cl and Table Cs and plotted in Figure Cl and Figure Cs. In the figures it can be seen that the

separation on the basis of size delineates different behaviors during at least 40 years following the earthquake. In that period, the shear strain rate in the small networks is roughly twice that of the regional networks. At around 40 years, strain rate in the smaller networks drops sharply to a level which is comparable to the average regional rate and (apparently) remains roughly constant until the present day.

The temporal behavior of the larger networks is quite different from that of the small near fault networks. Few of the regional strain estimates prior to 70 years are significantly different from zero (Figure Cl (a)). This does not mean that the strain rate was zero, only that nothing can be discerned with confidence about its nature prior to the most recent estimates. It can be noted that regionally ψ has been parallel to the strike of the SAF (Figure Cl (b)). The 1948-1963 estimate of Gilbert et al. (1992 in press) is not exceptional in its magnitude given the error envelope; however, the orientation is problematic.

The near fault networks from the Central 1906 show consistently significant shear strains rates over their entire history (Figure Cs (a)). ψ in these networks is also consistently fault parallel (Figure Cs (b)). The two non-zero points in Figure Cs (b) are from Point Arena (9.5 years) and Shelter Cove (47 years). Those points are parallel to the local faulting and reflect the fact that the SAF bends as it goes off shore at Point Arena (Curray and Nason 1967) . There is the suggestion of a temporal trend in the remaining points; if real, that trend would imply that ψ rotates to the west with time. The slope of a line fit to those data is -0.16 ± 0.11 deg/yr.

Table Cl. Strain rate estimates from the large networks of the Central 1906 segment (Figure 1).

Larger Network Results

Time since 1906	Length of interval	$\dot{\gamma}$	ψ	Source
8.5	7.5	0.79 ± 0.23	-41.0 ± 10.0	(Thatcher 1975) ; Primary Arc
19.5	3.5	0.55 ± 0.63	-65.8 ± 53.7	(Gilbert et al. 1992 in press) ; Coast Ranges
28	4	0.63 ± 0.39	-43.0 ± 19.0	(Thatcher 1975) ; Petaluma
29	13	0.46 ± 0.17	-36.0 ± 13.0	(Thatcher 1975) ; Primary Arc
32.5	9.5	1.00 ± 0.43	-76.7 ± 11.8	(Gilbert et al. 1992 in press) ; Coast Ranges
49.5	7.5	1.37 ± 0.75	-24.6 ± 7.8	(Gilbert et al. 1992 in press) ; Coast Ranges
71	14	0.41 ± 0.09	-73.7 ± 11.4	(Gilbert et al. 1992 in press) ; Coast Ranges
75	8	0.34 ± 0.02	-34.4 ± 1.5	(Lisowski et al. 1991) ; North Bay

Table Cs. Strain rate estimates from the small networks of the Central 1906 segment (Figure 1).

Near-Fault Small Network Results

Time	Length	$\dot{\gamma}$	ψ	Source

since 1906	of interval						
9.5	9.5	2.27	±	0.50	-17.7	± 5.9	(Thatcher 1975) ; Point Arena
12	12	2.41	±	0.80	-33.1	± 8.2	(Thatcher 1975) ; Fort Ross
28	4	2.22	±	0.63	-34.8	± 8.9	(Thatcher 1975); Pt.Reyes C
28	4	2.21	±	0.73	-32.8	± 10.0	(Thatcher 1975) ; Point Reyes
43.5	11.5	0.64	±	0.19	-38.5	± 9.1	(Thatcher 1975) ; Pt.Reyes C
43.5	11.5	0.56	±	0.16	-37.6	± 8.9	(Thatcher 1975) ; Point Reyes
43.5	19.5	0.31	±	1.08	-40.7	± 59.8	(Thatcher 1975) ; Fort Ross
47	23	1.01	±	0.18	-13.2	± 4.5	(Snay and Cline 1980) ; Shelter Cove
71.5	5.5	0.64	±	0.07	-43.1	± 2.3	(Prescott and Yu 1986) ; Point Reyes

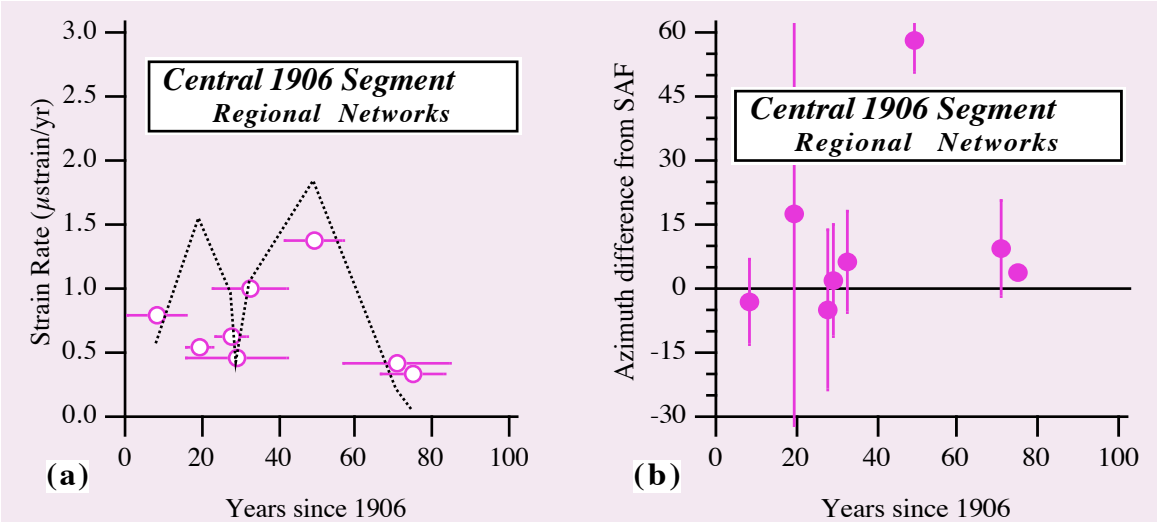

Figure Cl: Results from the regional networks of the Central 1906 segment. a) $\dot{\gamma}$, the dotted line is the 95% confidence level for the hypothesis that $\dot{\gamma}$ reflects only noise. b) Difference between ψ and strike of the SAF (N38W) with 1σ error bars.

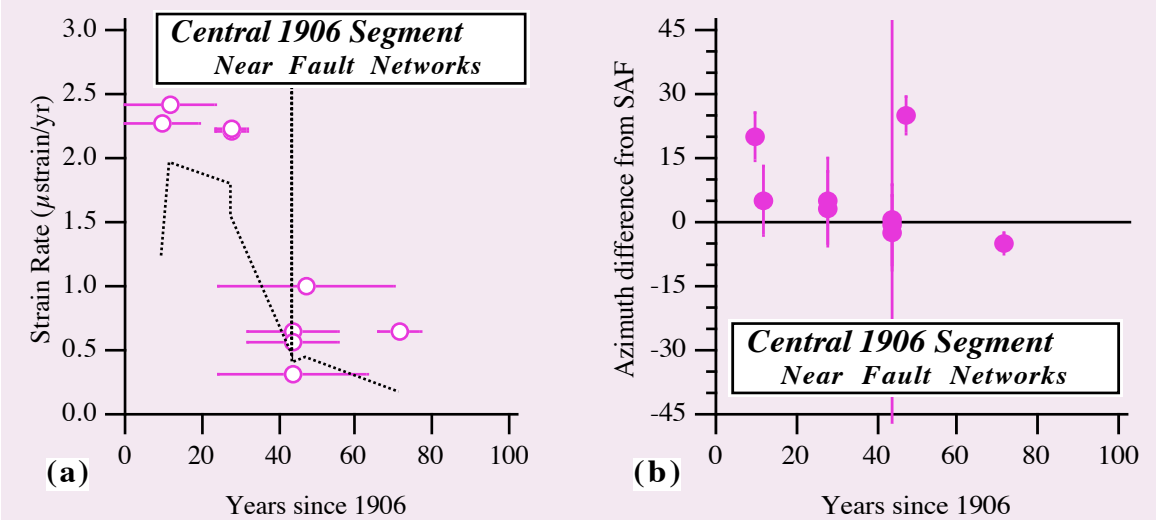

Figure Cs: Results from the near fault networks of the Central 1906 segment. a) $\dot{\gamma}$, the dotted line is the 95% confidence level for the hypothesis that $\dot{\gamma}$ reflects only noise. The spike at 43.5 years reflects a large error associated with one of the estimates for that time. b) Difference between ψ and strike of the SAF (N38W) with 1σ error bars.

Table PRP and Figure PRP contain results from the Point Reyes - Petaluma Arc (Figure 1). Figure PRP is analogous to Thatcher's (1975) Figure 6 but with $\dot{\gamma}$ and ψ plotted instead of $\dot{\gamma}_1$ and $\dot{\gamma}_2$. In the earlier epoch, 1930-1938, only the strain rate in the polygon which crosses the SAF is significantly different from zero; although in general the rates seem to be higher than those of the later epoch. In the later epoch, 1938-1961, strain rates are dramatically lower. In this epoch significantly nonzero strains occur only in polygons which cross mapped faults, the SAF on the west and the Rogers Creek on the east.

In the azimuth results the most striking observation that can be made is that the orientation of strain in the SAF crossing polygon is the only one which is unquestionably fault parallel (Figure PRP (b)). In the 1938-1961 results there is a suggestion of a spatial rotation of the direction of maximum shear as the Rogers Creek fault is approached but the magnitude of the errors prohibits any definite statement.

Table PRP: Strain rate results from the Point Reyes - Petaluma Arc (Thatcher 1975) .

Region	Distance from SAF	$\dot{\gamma}$	ψ
1930 - 1938			
A	-11	0.91 ± 3.30	-103.32 ± 118.91
B	-4	2.26 ± 2.46	3.89 ± 92.63
C	3	2.22 ± 0.63	-34.78 ± 8.90
D	13	2.34 ± 1.24	17.46 ± 11.13
E	19	0.97 ± 0.87	-28.44 ± 31.31
F	24	1.86 ± 1.29	12.96 ± 33.07

G	29	0.62 ± 0.81	-48.78 ± 39.61
H	33	0.18 ± 0.81	-31.72 ± 111.79
I	42	2.00 ± 0.78	-88.84 ± 60.90
1938 - 1961			
A	-11	0.83 ± 0.51	-60.78 ± 23.10
B	-4	0.33 ± 0.72	-2.38 ± 154.52
C	3	0.64 ± 0.19	-38.47 ± 9.09
D	13	0.27 ± 0.21	10.40 ± 47.98
E	19	0.15 ± 0.22	5.44 ± 169.58
F	24	0.25 ± 0.17	-36.45 ± 103.67
G	29	0.52 ± 0.21	-54.85 ± 20.50
H	33	0.70 ± 0.21	-71.82 ± 37.27
I	42	0.30 ± 0.19	12.19 ± 152.02

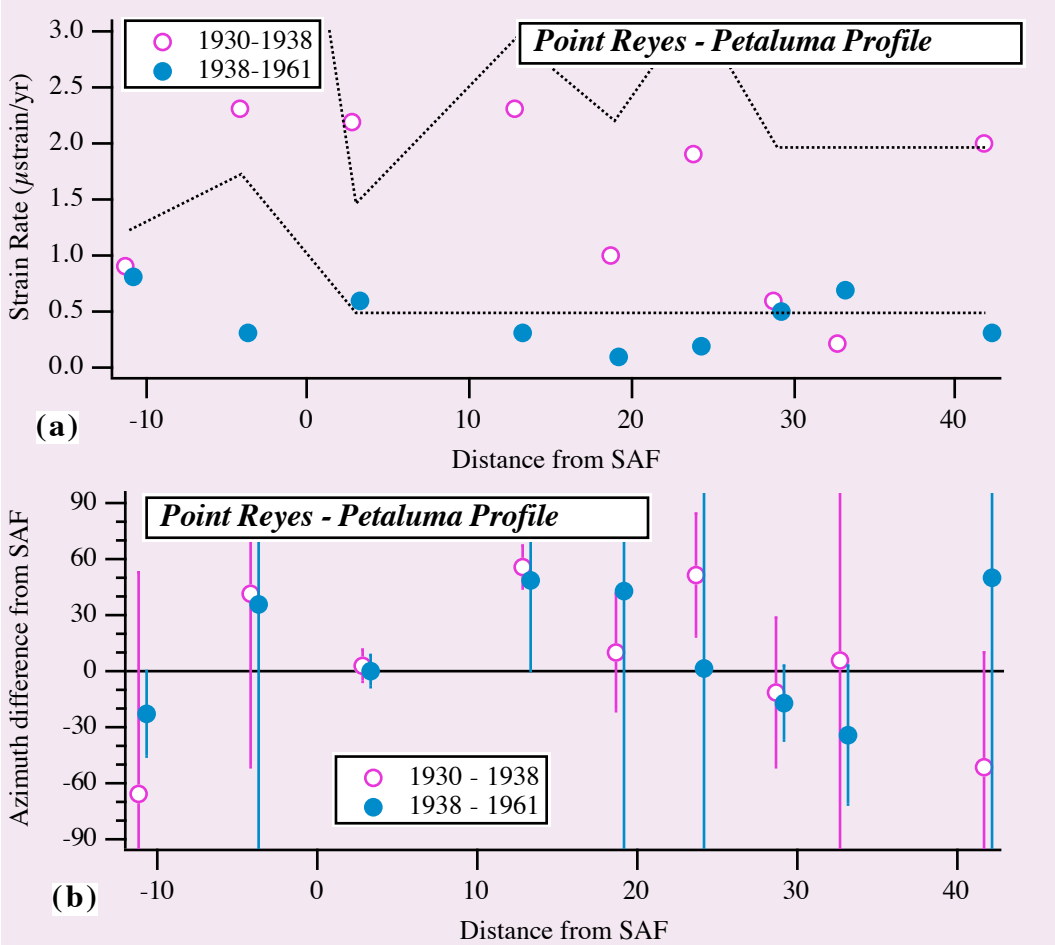

Figure PRP: Profiles from the Point Reyes-Petaluma arc. These results are computed from the γ_1 and γ_2 values computed from the data by Thatcher (1975) . a) $\dot{\gamma}$, the dotted line is the 95% confidence level for the hypothesis that $\dot{\gamma}$ reflects only noise. b) ψ with 1σ error bars.

Hayward Network

The earliest results for the Hayward network are from triangulation data of the 1951-1957 epoch (Thatcher 1975) . Shortly after the triangulation measurements were begun, some of the earliest trilateration measurements were made in this region (Hoffman 1968) ; thus the network has both triangulation and trilateration measurements throughout its early history. All of the available results are presented in Table HY and Figure HY. With the exception of a single triangulation result, the Hayward network shows consistently significant shear strain rate and that rate appears to decrease with time since the beginning of the history of that net. ψ is fairly constant and parallel to the N25W strike of the Calaveras fault which strikes 10 degrees more northerly than the ~N35W strikes of the Hayward and SAF (Jennings 1975) . In these results there is a suggestion of a westward rotation of ψ similar to that of the near fault results of the Central 1906 segment (Figure Cs (a)). The implied rate here is some what higher at -0.45 ± 0.21 deg/yr.

Table HY: Strain rate estimates from the Hayward network.

Hayward Net Results

Year	Length of interval	$\dot{\gamma}$	ψ	Source
1954	6	1.02 ± 0.39	-21.0 ± 16.0	(Thatcher 1975) ; Whole net
1960	6	0.55 ± 0.25	-13.0 ± 18.0	(Thatcher 1975) ; Whole net
1964	7	0.87 ± 0.10	-24.0 ± 4.0	(Prescott et al. 1981) ; CDWR network
1975	10	0.42 ± 0.02	-26.0 ± 2.0	(Prescott et al. 1981) ; CDWR network
1975	10	0.26 ± 0.02	-35.0 ± 4.0	(Prescott et al. 1981) ; East Bay
1981	16	0.38 ± 0.02	-31.0 ± 1.6	(Lisowski et al. 1991) ; S + Cent SF Bay

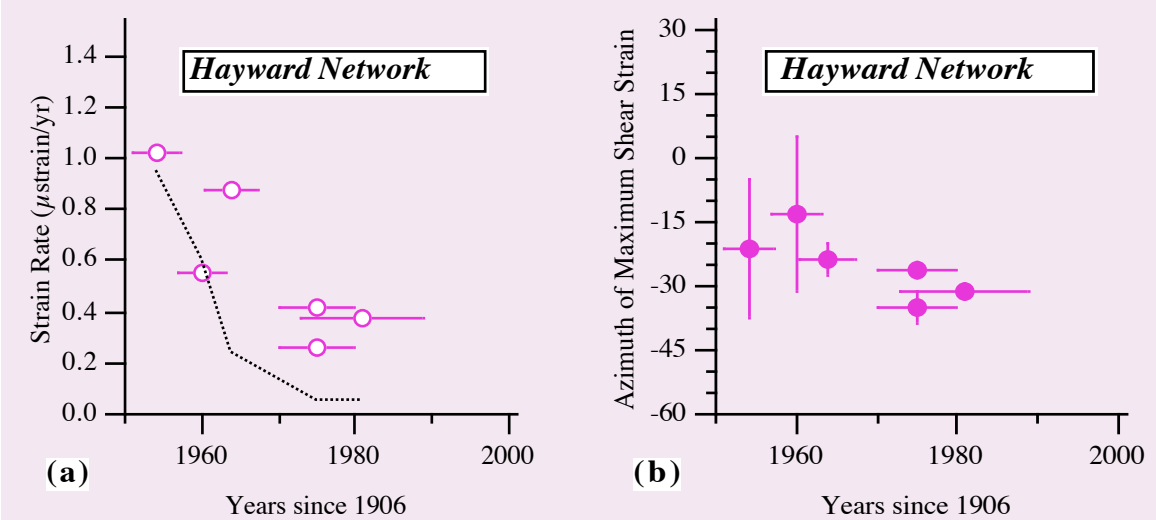

Figure HY: Results from the Hayward Network. a) $\dot{\gamma}$, the dotted line is the 95% confidence level for the hypothesis that $\dot{\gamma}$ reflects only noise. b) ψ with 1σ error bars.

In the early trilateration history, the technique and technology were evolving; thus there is some concern in the literature that changes in rate early in the trilateration history may be due to technique changes rather than tectonics. In particular, the significance of the difference between the 1963.5 and 1975 results has been questioned by Prescott et al. (1981) . Measurements for the 1963.5 result were made by the California Department of Water Resources (CDWR) between 1960 and 1967. Following 1967, the measurement technique changed and the responsibility for monitoring this network was taken over by the California Division of Mines and Geology (CDMG). In 1968 the USGS took over responsibility for monitoring but the measurement technique did not change (Prescott et al. 1981) . Prescott et al. (1981) dismiss the significantly higher earlier rate as spurious because the change in rate occurs with the change in measurement technique. The coincidence is unsettling and certainly unfortunate, but in the context of Figure HY that point does not look terribly out of place.

Using Frank's method, Thatcher (1975) computed shear strains for a spatial profile across the Hayward net. Those results are presented in Table HP and Figure HP. Figure HP reveals no convincing across-strike variability; although the two polygons closest to the SAF seem to straining at a higher rate than the two easternmost polygons.

Table HP: Strain rate estimates from the Hayward Arc profile (Thatcher 1975) .

Distance	$\dot{\gamma}$	ψ
13.0	0.86 ± 0.27	-13.49 ± 33.06
30.0	1.10 ± 0.30	-21.47 ± 11.58
48.5	0.63 ± 0.22	4.73 ± 118.79
67.0	0.60 ± 0.39	-41.70 ± 17.79

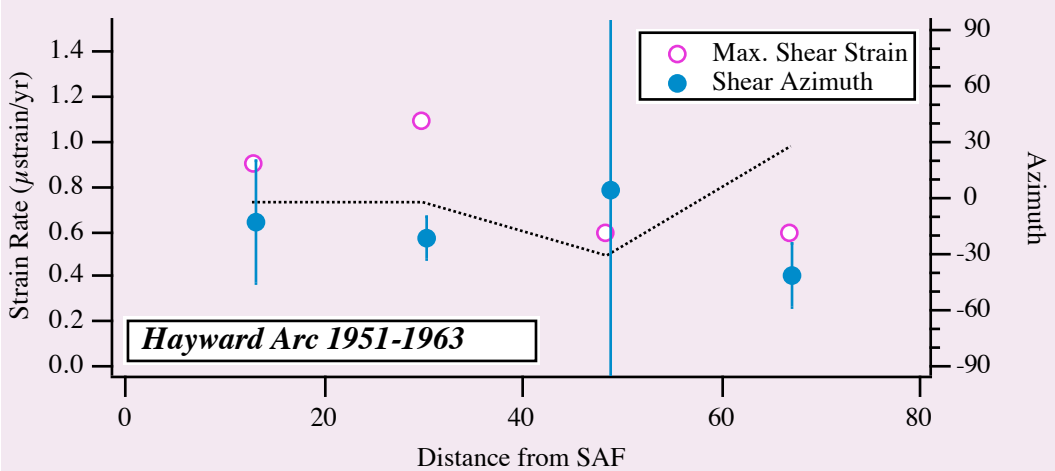

Figure HP: A spatial profile across the Hayward net. The data for this profile are from Thatcher (1975) . The eastern 2 points are east of the Hayward fault. The dotted line marks the 95% confidence level for the hypothesis the $\dot{\gamma}$ reflects only noise.

In Figure NH, results from both of the large networks (Primary Arc and Hayward net) have been plotted. It must be borne in mind that there is considerable variability in tectonic style throughout the region represented by those results; however the similarity of the values for $\dot{\gamma}$ and ψ reported by Lisowski et al. (1991) (Table T) lend support to the notion that the combination presented in Figure NH is reasonable. The most striking aspect of Figure NH is the dramatic reduction of the size of the associated errors with the introduction of trilateration at around 60 years. The triangulation results of the first 60 years or so do very little to constrain the regional average of strain.

The results for ψ certainly do not rule of the hypothesis that the regional strain field has been parallel to the SAF throughout the time since the 1906 event; however the Hayward network data seem to have been oriented slightly more to the east (as would be expected if the Calaveras fault is exerting an influence in the area) than the data from the north. In recent years the two fields have been quite similar in both rate and orientation.

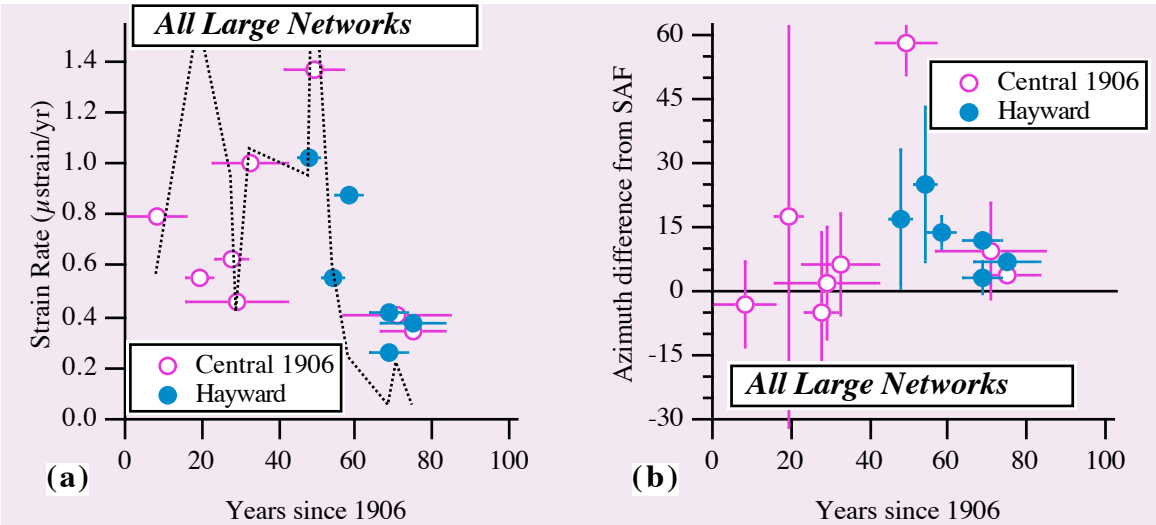

Figure NH: Central 1906 (Table Cl) and Hayward Net (Table HY) results plotted together. a) $\dot{\gamma}$, the dotted line is the 95% confidence level for the hypothesis that $\dot{\gamma}$ reflects only noise. b) ψ with 1σ error bars.

Residuals

Models; slight return

In several of the reports of results from Study Area, anomalous results are reported. Results thus characterized are ones which cannot be predicted by the preferred model and in the context of Eqn. 0a, they are residuals. Also from Eqn 0a, two ways of explaining an anomalous result can be seen; either the data are erroneous or the chosen model needs revision. As noted by several authors (e.g. Kuhn (1970) and Feyerabend (1988)), models are deeply ingrained within any given scientific community; thus the preferred explanation for any anomalous result is that the measurements and/or the processing which lead to it are in error. Indeed it is this preference which guarantees that progress can be made; it ensures that genuine blunders are ferreted out and identified. Despite the most conscientious efforts at eliminating such errors some anomalies will always remain and it is these results which point the way for improving our understanding.

Dilatations

The most insidious anomaly is an excursion in the dilatation. This sort of anomaly can result from systematic measurement error as well as from tectonic causes. Systematic measurement errors are isotropic and will affect both strain components; thus they will not affect the shear ($\varepsilon_{11} - \varepsilon_{22}$) but will turn up as a change in dilatation ($\varepsilon_{11} + \varepsilon_{22}$). It is this characteristic which makes detection of isotropic tectonic dilatations extremely difficult. Conscientious measurement practice coupled with the absence of an obvious tectonic model require that the default assumption concerning dilatations be that they are the result of systematic error.

Prescott et al. (1981) report an anomalous dilatation event in the Calaveras Lake (Figure 1) results which corresponds with an anomaly in γ_1. The correspondence between the dilatation and γ_1 allows systematic measurement error to be ruled out and the authors attribute the results to an episode of uniaxial E-W contraction. The episode must have been aseismic as there is no contemporaneous nearby seismicity which could have been responsible.

A truly baffling dilatation anomaly is reported in the Hollister net by Savage et al. (1979) . They note that in 1973 and 1974 the network underwent an anomalous increase in the dilatation rate. A similar anomaly was noted in the Palmdale network 350 km to the south. The correlation between the Hollister and Palmdale anomalies strongly suggested that a systematic measurement error was at the source; however, when the components of strain at Hollister were examined closely it was found that the anomaly there was primarily caused by an excursion in ε_{11} and that ε_{22} changed at a fairly constant rate. As noted above, if the anomalies were due to systematic measurement error, the dilatation would be manifested as an change in both components. The results instead suggest that the dilatation is due to an anisotropic E-W extension. In the original investigation the authors, while acknowledging the anisotropy of the principal components, preferred an unidentified systematic measurement error as the explanation.

Savage et al. (1981) returned to the problem of unidentified systematic measurement error and the coherence between Hollister and Palmdale dilatations. In this later paper a thorough consideration of the systematic error in the USGS measurement system is reported. There is no appreciable drift relative to daily measurements made with a multi-wavelength distance-measuring device and it is noted that dilatations in other networks (in southern California) are not correlated to the degree of the Palmdale and Hollister networks. The authors conclude that systematic errors are adequately quantified in their error estimates. This conclusion seems to support a tectonic interpretation of the 1973-1974 event in the Hollister network. An unstated corollary of this conclusion is that dilatations which are coherent over spatial scales of 100's of kilometers may be a real tectonic phenomena in California.

Prescott et al. (1981) report that a large number of lines in the East Bay show an apparent lengthening in April-May 1980. This event follows the Livermore earthquakes of January 1980 but is unlikely to be related to those earthquakes because of the wide areal extent of the affected lines. While this is not explicitly reported as a dilatation anomaly, it has all of the characteristics of such an event.

Changes in Rate

The most striking anomaly of this type occurs in the Mocho net (Figure 1) (Prescott et al. 1979) . As of Prescott et al.'s writing, this network had been surveyed three times (1973, 1975 and 1978). 75% of the strain measured between 1973 and 1978 occurred during the 1973-1975 epoch; this implies that the strain rate in the 1975-1978

period was ~10% of the preceding epoch. Prescott et al. (1979) report that they have no reason to suspect their measurements, but they have no tectonic explanation either.

Savage et al. (1979) report that deformation across the Hollister network did not occur at a constant rate in the epoch 1971-1978. Relative to the average, deformation rates were elevated in the years 1973-1974 and depressed in the years 1975-1976. The increased rate corresponds closely with the anomalous ε_{11} results discussed above.

Prescott and Yu (1986) report larger than expected fault normal velocities at 6 of their 39 stations. Of these, three are geometrically weak determinations and a fourth is in a geothermal field. The remaining two are close to the SAF and are dismissed as only marginally significant.

In addition to the short excursions outlined above there is a longer term change in rate represented by the data from the Hayward Arc. Since it's first measurement in the 1950's the shear strain rate in that network has been decaying (Figure HY). The change in rate there was first noticed by Pope et al. (1966) . It was noted at that time that the displacements in the years 1951-1957 vastly exceeded those of the following epoch (1957-1963). Thatcher (1975) reported that the strain rate in the first epoch was higher than that of the second but the difference was less that his 2σ error and it was dismissed as insignificant. In considering Thatcher's results, Savage and Burford (1973) attributed the difference to error in the measurement of the azimuth between Diablo and Mocho in 1951, but Whitten (1959) casts doubt on that being the cause, "Check angles which were measured at each end of the base indicated that adverse conditions did not exist ..." In the context of Figure HY it would seem that indeed Thatcher's points are significantly different. The first is above the 95% confidence level while the second is below it; thus the first is greater than zero and the second need not be.

Early 1960's CDWR trilateration data from the East Bay also show abnormal behavior. Savage and Burford (1973) note that line lengths measured from Diablo between 1960 and 1970 are inconsistent with "any simple interpretation" (station names for Savage and Burford's data are given in Hoffman (1968)). The high strain rate indicated by CDWR trilateration data discussed above (Figure HY) is also from this area and spans the years 1960-1967.

Coincident with the elevated Hayward and CDWR rates is the anomalous result of 1948-1963 presented by Gilbert et al. (1992 in press) . If real, that result indicates a dramatic change in the orientation of the strain field and an elevated strain rate; however the large errors associated with that point leave it within the bounds of expected statistical fluctuation and it need not be associated with any tectonic processes.

Discussion

Let me now turn to the two big boxes which gave rise to this paper, Pac:Nam and the earthquake cycle. Pac:Nam is the boundary between North America and the Pacific plate. In the strict plate tectonic model that boundary is narrow and separates the rigid

Pacific and North American plates. While rigid interiors are still popular, it is now generally agreed that the narrow part of the plate tectonic definition should be dropped, at least in the case of continental strike-slip boundaries. We now consider Pac:Nam to be a system of faults related to the SAF with the SAF as the main player. Faults (as opposed to folding and penetrative mechanisms) remain at the center of our attention as far as Pac:Nam deformation is concerned.

I suggest that another definition for a plate boundary might be "the region spanned by a gradient in velocity between two regions of nearly constant velocity". In this model Pac:Nam is the area between regions with velocities like the mid-Pacific and regions with velocities like the eastern United States. This definition stems from observations rather than from paradigm. One advantage of this is that there are no a priori models of how the associated deformation should be distributed. We know that the gradient exists, we are less sure of exact mechanism of its generation. In addition to the fundamental result of its existence, the velocity gradient between the Pacific and North America seems to have some structure. Consider the sequence of scales represented by Ward (1990) , Argus and Gordon (1991) and Lisowski et al. (1991) ; Ward observes what could easily be a smooth gradient extending from the SAF to the Rockies, Argus and Gordon consider the important that gradient to have two parts, separated by the Sierra Nevada batholith, and Lisowski et al. consider the important part to be the (roughly) smoothly varying gradient associated with the faults of the SAF system. In southern California velocity gradients detected with geodetic data have been used to propose the existence of hither-to undetected zones relative horizontal movement.

Another advantage of the velocity gradient definition for plate boundaries is that it does not run into semantic difficulties at small scales. As our understanding of the distribution of deformation related to relative motions of the surface of Earth becomes deeper, it has been necessary to postulate smaller and smaller plates. Some of the smallest plates have widths which are comparable (or smaller even) than the plate thickness. Equidimensional "plates" are a semantic difficulty because it is not clear that there is a difference between the boundary and the interior. The velocity gradient definition avoids such difficulty by making no assertions concerning scale; gradients can exist on whatever scale one chooses to measure.

Study Area is only a portion of the SAF system, yet even within that box the deformation field associated with Pac:Nam evolves from south to north. In the south, near Hollister, the deformation is concentrated close to the SAF and is quite narrow; the velocity gradient is quite steep. As the Calaveras and SAF diverge, the deformation becomes more complex. Deformation associated with the Calaveras is dominated by creeping mechanisms; that associated with the SAF is more like that expected within EM. Further north, in the networks just south of San Francisco, the Calaveras fault spawns the Hayward fault. There are no obvious tears in velocity profiles across the region (Lisowski et al. 1991) , but Prescott et al. (1981) conclude that strain need not be

accumulating in the East Bay. Finally in the North Bay the deformation field extends at least 80 km to the east from the SAF and all the faults in the region appear to be locked; the velocity gradient is considerably more gentle than to the south. In general there is a progressive broadening of the field and locking of the faults from south to north within Study Area. While we do not have detailed measurements from Point Arena or Shelter Cove, results for ψ from those networks suggest that the northernmost regions of Study Area could be considered in a box of their own.

While models such as EM and VEM do an adequate job of modeling the available results, their spirit denies any along-strike heterogeneity. Such heterogeneity is a first order characteristic of Pac:Nam and of Study Area (Figure 0 and Figure 1). It may be reasonable to assume homogeneity within any particular network but the application of EM or VEM in such a situation denies that the network is a box. The boundaries of that box have often been chosen exactly because of heterogeneities; thus within Study Area, the along-strike extrapolation beyond the boundaries of network-size boxes (the uniform, homogeneous, linear meta-model) implied by model classes such as VEM and EM is not necessarily trivial.

Another thing that we know about Pac:Nam is that its associated deformation often makes itself known in the form of earthquakes along the SAF system. We know that segments of Pac:Nam have experienced several earthquakes of similar character throughout their history and we believe that the earthquakes of such sequences are cyclic.

"Cyclic earthquakes" is a model of the recurrence of earthquakes that asserts that there is a causal relationship between the occurrence of an earthquake and some sequence of physical events which repeats itself before each earthquake. The details of that sequence may vary, but we believe that, at some level, it exists; furthermore, we believe that it is possible to know that sequence and that if it is known that we will be better able to predict the occurrence of future earthquakes. This belief reflects the very core of western rational thought; the separation of cause and effect. It is almost inconceivable that earthquakes could recur without some repeating causal mechanism. It is this belief which has been the driving force behind this paper. If such a cycle exists, the results above should reflect its character and provide information about the sequence of events between earthquakes.

Results from the small near fault networks of the Central 1906 segment (Figure Cs) are the only results which show an unequivocal variation in strain rate throughout their history. Results from the Hayward network (Figure HY) also show temporal variation but there is debate concerning the data from that network; thus the results can not be considered unequivocal. The contrast between the near fault data (Figure Cs) and the regional data (Figure Cl) from the Central 1906 segment suggests that strain may be concentrated along the SAF at least in the early part of the cycle. In the context of EM, this would imply a shallow value for D. The abrupt decrease in the near fault rate around 40 years (Figure Cs) would require that D deepen suddenly around that time. The errors

associated with the results of Figure Cs (Table Cs) are such that it is possible that the abrupt change in strain rate is only apparent; if this is the case, Thatcher (1983) has shown that those data are consistent models of the VEM class (Figure VEM).

The noise level of the results from the regional networks (Figure NH) makes it difficult to generalize about temporal variability at that scale. The significantly non-zero points in that subset do not form any obvious pattern but any of a constant rate, a slow decay or an abrupt change around 60 years might be entertained. Occam's razor would dictate a constant rate at the regional scale. In a linear world, a constant rate at regional scales and a varying rate at local scales suggests that the process(es) at the local level are on top of a background process. Thatcher's (1983) post-seismic rebound on top of some constant regional strain field is one such possibility. Reches and Schubert (1992 in press) also compute variations on top of an ongoing regional strain. Whatever the details, such a separation of regional and local process implies either that there are two independent processes with unique scales or that there is a single process whose effects vary with the scale of observation.

A generalization which can be made within Study Area and which is consistent with results from beyond as well is that ψ tends to be parallel to the local faulting (Prescott et al. 1979; Prescott and Yu 1986; Lisowski et al. 1991) . In most cases this is the direction of the SAF; but in cases such as the East Bay or Napa networks the correspondence is best if the strike of the Calaveras or Green Valley faults is used. This relationship between ψ and the direction of local faulting implies that a causal link between the two exists. It is easiest to imagine that the local faulting is controlling the direction of maximum shear strain through the deformation mechanism of simple shear across the faults. In regions where the strike of the faulting is variable, such as the North Bay and East Bay, this in turn suggests that interaction between faults is small. The planar discontinuities of models such as EM' are more conducive to this sort of isolation than the horizontally extensive viscoelastic layer of VEM type models.

The near fault results (Figure Cs) and the results from the Hayward network (Figure HY) suggest that in some cases ψ exhibits modest temporal variation around the local fault direction. In the case of the Hayward results, the temporal variation is from an orientation roughly parallel to the Calaveras to one which is roughly parallel to the SAF. In the Central 1906 segment, the variation is about a mean SAF direction. In the current models of the earthquake cycle, any strain which is not fault parallel is residual; it follows that temporal variability of ψ also cannot be accounted for. Such effects are second order compared to the large fault parallel component but it is not unreasonable to consider the implications of their existence.

Summary

Science is an attempt to understand the world around us; to make progress in that endeavor we divide the large problems into smaller, manageable problems. We solve

those problems by making analogies between processes which are understood and those which are not. How problems are divided and analogies chosen determines what will be know and what will remain a mystery. The very act of drawing a box or of making an analogy ensures that some mystery concerning the workings of the world will always remain.

This paper has focused on the region immediately surrounding the portion of the SAF which ruptured in 1906; it has an emphasis on areas ~75 km north and south of San Francisco. Within this box, the spatial distribution of strain evolves from a narrow concentrated zone near Hollister through a complex zone of mixed style, to a broad distributed zone north of San Francisco. Estimates of strain rate from networks with regional extent suggest that strain rate has remained constant since the 1906 earthquake, but the results are quite noisy and it is not reasonable to make definite statements. Strain rates near the fault do show temporal variability and, in the early years after the 1906 earthquake, were significantly elevated compared to the regional rates. To first order, the direction of maximum shear strain is parallel to local faulting everywhere; this is taken to imply that the faults control the orientation of the strain field. It is suggested that perhaps models such as EM would allow the necessary regional variation more easily than models analogous to VEM. Some second order temporal variation in the orientation of the strain field about the faulting directions is also noted; this variation is not present in any of the available models.

"*Mu*"

Appendix 1 - Error Propagation

Error propagation for γ

Let the error associated with γ_1 be σ_1 and the error associated with γ_2 be σ_2. From Taylor (1982,, eqn. 3.26) the error associated with $q = x^n$ is

$$\sigma_q = (n\, \sigma_x \mid q \mid) / \mid x \mid \qquad \text{(A1.1}$$

thus the error associated with γ_1^2 is

$$\sigma_{\gamma_1^2} = 2\, \gamma_1\, \sigma_{\gamma_1} \qquad \text{(A1.2}$$

and the error associate with γ_2^2 is

$$\sigma_{\gamma_2^2} = 2\, \gamma_2\, \sigma_{\gamma_2} \qquad \text{(A1.3}$$

To get the error associated with γ, σ_1 and σ_2 must be propagated through

$$\gamma = (\gamma_1^2 + \gamma_2^2)^{1/2} \qquad \text{(A1.4}$$

From Taylor (1982,, eqn. 3.16) an expression for the error associated with γ^2 is

$$\sigma_{\gamma^2} = \left(\sigma_{\gamma_1^2}^2 + \sigma_{\gamma_2^2}^2 \right)^{1/2} \qquad \text{(A1.5}$$

and again following Taylor's eqn. 3.26

$$\sigma_\gamma = \frac{\sigma_{\gamma^2}}{2\,\gamma} \qquad \text{(A1.6}$$

Doing the appropriate substitutions

$$\sigma_\gamma = \frac{1}{\gamma} \left(\gamma_1^2 \sigma_1^2 + \gamma_2^2 \sigma_2^2 \right)^{1/2} \qquad \text{(A1.7}$$

Error Propagation for ψ

The relationship between ψ and γ_1 and γ_2 is

$$\psi(\gamma_1,\gamma_2) = 1/2 \tan^{-1} (-\gamma_2/\gamma_1) \qquad \text{(A1.8}$$

Assuming that γ_1 and γ_2 are independent, from Taylor (1982,, eqn. 9.3)

$$\sigma_\psi = \left[\left(\frac{\partial \psi(\gamma_1,\gamma_2)}{\partial \gamma_1}\, \sigma_1 \right)^2 + \left(\frac{\partial \psi(\gamma_1,\gamma_2)}{\partial \gamma_2}\, \sigma_2 \right)^2 \right]^{1/2} \qquad \text{(A1.9}$$

Doing the algebra gives

$$\sigma_\psi = \left[\frac{\gamma_2^2 \sigma_1^2}{\gamma_1^4} + \gamma_1^2 \sigma_2^2 \right]^{1/2} \qquad \text{(A1.10}$$

Appendix 2 - Bias associated with γ

If σ_1 and σ_2 are approximately equal, then γ^2 (Eqn A1.4) is chi-square distributed and γ will be Rayleigh distributed (Bendat and Piersol 1966, p.129) . The probability of finding a given value of γ is

$$p(\gamma) = \frac{\gamma}{\sigma_\gamma^2} \exp\left(\frac{-\gamma^2}{2\sigma_\gamma^2}\right) \qquad \text{(A2.1}$$

(Bendat and Piersol 1966, eqn. 7.20) . The probability that γ is between 0 and some value x is

$$P(0 < \gamma < x) = \int_0^x p(\gamma)\, d\gamma \qquad \text{(A2.2}$$

In this paper, it is the value of x which is associated with some value of P which is desired. This is found by construction. For each estimate of γ, Eqn. A2.1 is integrated numerically and the value of x is found by computer search.

References

Argus, D. F. and Gordon, R. G. (1991). Current Sierra Nevada - North America motion from very long baseline interferometry: Implications for the kinematics of the western U.S. *Geology* **19**: 1085-1088.

Beloussov, V. V. (1990). Tectonosphere of the Earth: upper mantle and crust interaction. *Tectonophysics* **180**: 139-183.

Bendat, J. S. and Piersol, A. G. (1966). *Measurement and analysis of random data*. New York, J. Wiley & Sons.

Carey, S. W. (1976). *The Expanding Earth*. New York, Elsevier.

Chamberlain, T. C. (1897). The method of multiple working hypotheses. *Journal of Geology* **5**: 837-848.

Curray, J. R. and Nason, R. D. (1967). San Andreas fault north of Point Arena, California. *Geological Society of America Bulletin* **78**: 413-418.

Feyerabend, P. (1988). *Against Method*. New York, Verso.

Frank, F. C. (1966). Deduction of Earth strains from survey data. *Bulletin of the Seismological Society of America* **56**(1): 35-42.

Gilbert, G. K. (1884). A theory of the earthquakes of the Great Basin, with a practical application. *American Journal of Science* **XXVII**(157): 49-53.

Gilbert, L. E., et al. (1992 in press). Analysis of a 100 year geodetic record from northern California.

Hoffman, R. B. (1968). Geodimeter fault movement investigations in California. California Department of Water Resources.

Hofstadter, D. R. (1980). *Gödel, Escher, Bach: an eternal golden braid*. New York, Vintage Books.

Isacks, B., et al. (1968). Seismology and the new global tectonics. *Journ. Geophys. Res.* **73**(18): 5855-5899.

Jennings, C. W. (1975). Fault Map of California. San Francisco, CA, California Division of Mines and Geology.

Kuhn, T. S. (1970). *The Structure of Scientific Revolutions.* Chicago, The University of Chicago Press.

Larson, K. M. and Agnew, D. C. (1991). Application of the Global Positioning System to crustal deformation measurement 1. precision and accuracy. *Journ. Geophys. Res.* **96**(B10): 16,547-16,565.

Lawson, A. L. (1908). The California Earthquake of April 18, 1906. Report of the State Earthquake Investigation Commission. Washington D.C., Carnigie Institution. **I:** 451.

Leick, A. (1990). *GPS Satellite Surveying*. New York, John Wiley & Sons.

Li, V. C. and Rice, J. R. (1987). Crustal deformation in great California earthquake cycles. *Journ. Geophys. Res.* **92**(B11): 11,533-11,551.

Lisowski, M., et al. (1991). The velocity field along the San Andreas fault. *Journ. Geophys. Res.* **96**: 8369-8389.

McKenzie, D. P. and Parker, R. L. (1967). The North Pacific: an example of tectonics on a sphere. *Nature* **216**: 1276-1280.

Oliver, J. (1987). Discovery and innovation in geoscience. *Geological Society of America Bulletin* **100**: 157-159.

Pope, A. J., et al. (1966). Surveys for crustal movement along the Hayward fault. *Bulletin of the Seismological Society of America* **56**(2): 317-323.

Popper, K. R. (1968). *Conjectures and Refutations: the growth of scientific knowledge*. New York, Harper Torchbooks.

Prescott, W. H. (1976). An extension of Frank's method from obtaining crustal shears strains from survey data. *Bulletin of the Seismological Society of America* **66**(6): 1847-1853.

Prescott, W. H. (1981). The determination of displacement fields from geodetic data along a strike slip fault. *Journ. Geophys. Res.* **86**(B7): 6067-6072.

Prescott, W. H., et al. (1981). Geodetic measurement of crustal deformation on the San Andreas, Hayward and Calaveras faults near San Francisco, California. *Journ. Geophys. Res.* **86**(B11): 10,853-10,869.

Prescott, W. H. and Nur, A. (1981). The accommodation of relative motion at depth on the San Andreas fault system in California. *Journ. Geophys. Res.* **86**(B2): 999-1004.

Prescott, W. H., et al. (1979). Strain accumulation rates in the western United States between 1970 and 1978. *Journ. Geophys. Res.* **84**(B10): 5423-5435.

Prescott, W. H. and Yu, S.-B. (1986). Geodetic measurement of horizontal deformation in the northern San Francisco Bay region, California. *Journal of Geophyscial Research* **91**(B7): 7475-7484.

Reches, Z. and Schubert, G. (1992 in press). A non-linear viscoelastic model of the earthquake cycle. :

Reid, H. F. (1910). The mechanics of the earthquake. The California Earthquake of April 18, 1906. Washington, D. C., Carnegie Inst. of Washington. **II:** 16-28.

Savage, J. C. (1990). Equivalent strike-slip earthquake cycles in half-space and lithosphere-asthenosphere earth models. *Journ. Geophys. Res.* **95**(B4): 4873-4879.

Savage, J. C. and Burford, R. O. (1970). Accumulation of tectonic strain in California. *Bulletin of the Seismological Society of America* **60**(6): 1877-1896.

Savage, J. C. and Burford, R. O. (1971). Discussion of paper by C.H. Scholz and T.J. Fitch, "Strain accumulation along the San Andreas fault". *Journ. Geophys. Res.* **76**(26): 6469-6479.

Savage, J. C. and Burford, R. O. (1973). Geodetic determination of relative plate motion in central California. *Journ. Geophys. Res.* **78**(5): 832-845.

Savage, J. C., et al. (1981). Strain accumulation near the epicenters of the 1978 Bishop and 1980 Mammoth Lakes, California, earthquakes. *Bulletin of the Seismological Society of America* **71**(2): 465-476.

Savage, J. C. and Prescott, W. H. (1978). Asthenosphere readjustment and the earthquake cycle. *Journ. Geophys. Res.* **83**(B7): 3369-3376.

Savage, J. C., et al. (1979). Deformation across the Salton Trough, California, 1973-1977. *Journ. Geophys. Res.* **84**(B6): 3069-3079.

Savage, J. C., et al. (1979). Geodolite measurements of deformation near Hollister, California, 1971-1978. *Journ. Geophys. Res.* **84**(B13): 7599-7615.

Savage, J. C., et al. (1981). Strain accumulation in southern California, 1973-1980. *Journ. Geophys. Res.* **86**(B8): 6991-7001.

Scholz, C. H. and Fitch, T. J. (1969). Strain accumulation along the San Andreas fault. Journ. Geophys. Res. 74(27): 6649-6666.

Snay, R. A. and Cline, M. W. (1980). Geodetically derived strain at Shelter Cove, California. *Bulletin of the Seismological Society of America* **70**(3): 893-901.

Taylor, J. R. (1982). *An introduction to error analysis: the study of uncertainties in physical measurements*. Mill Valley, Ca, University Science Books.

Thatcher, W. (1975). Strain accumulation and release mechanism of the 1906 San Francisco earthquake. *Journ. Geophys. Res.* **80**(35): 4862-4872.

Thatcher, W. (1975). Strain accumulation on the northern San Andreas fault zone since 1906. *Journ. Geophys. Res.* **80**(35): 4873-4880.

Thatcher, W. (1983). Nonlinear strain buildup and the earthquake cycle on the San Andreas fault. *Journ. Geophys. Res.* **88**(B7): 5893-5902.

Ward, S. (1990). Pacific-North American plate motions: new results from very long baseline interferometry. *Journ. Geophys. Res.* **95**: 21,965-21,981.

Whitten, C. A. (1959). Notes on remeasurement of triangulation net in the vicinity of San Francisco. *California Division of Mines and Geology, Special Report* **57**: 56-57.